High-throughput density functional calculations to optimize properties and interfacial chemistry of piezoelectric materials

Jordan A. Barr,[1] Fang-Yin Lin,[2] Michael Ashton,[2] Richard G. Hennig,[2] and Susan B. Sinnott[1,*]

[1]*Department of Materials Science and Engineering, The Pennsylvania State University, University Park, Pennsylvania 16801, USA*

[2]*Department of Materials Science and Engineering, The University of Florida, Gainesville, Florida 32611, USA*

(Received 10 June 2017; revised manuscript received 23 December 2017; published 28 February 2018)

High-throughput density functional theory calculations are conducted to search through 1572 ABO_3 compounds to find a potential replacement material for lead zirconate titanate (PZT) that exhibits the same excellent piezoelectric properties as PZT and lacks both its use of the toxic element lead (Pb) and the formation of secondary alloy phases with platinum (Pt) electrodes. The first screening criterion employed a search through the Materials Project database to find *A*-*B* combinations that do not form ternary compounds with Pt. The second screening criterion aimed to eliminate potential candidates through first-principles calculations of their electronic structure, in which compounds with a band gap of 0.25 eV or higher were retained. Third, thermodynamic stability calculations were used to compare the candidates in a Pt environment to compounds already calculated to be stable within the Materials Project. Formation energies below or equal to 100 meV/atom were considered to be thermodynamically stable. The fourth screening criterion employed lattice misfit to identify those candidate perovskites that have low misfit with the Pt electrode and high misfit of potential secondary phases that can be formed when Pt alloys with the different *A* and *B* components. To aid in the final analysis, dynamic stability calculations were used to determine those perovskites that have dynamic instabilities that favor the ferroelectric distortion. Analysis of the data finds three perovskites warranting further investigation: $CsNbO_3$, $RbNbO_3$, and $CsTaO_3$.

DOI: 10.1103/PhysRevMaterials.2.025002

I. INTRODUCTION

Lead zirconate titanate (PZT) has desirable piezoelectric properties that have led to its use in numerous technological applications including sensors, actuators, field-effect transistors, and memory applications [1–4]. The piezoelectric properties are enhanced due to the existence of a morphotropic phase boundary (MPB) between the ferroelectric tetragonal and rhombohedral phases, in which the polarization vector has many possible directions, allowing for an almost continuous rotation through the two phases [5,6]. Despite possessing excellent piezoelectric properties, there are challenges associated with the use of PZT in these applications. Of these challenges, one is the increasing push to eliminate the use of lead-based compounds due to the toxicity of lead. In addition, there is substantial evidence that when PZT is in contact with metal electrodes, in particular platinum (Pt) electrodes, secondary phases such as Pt_3Pb and Pt_3Ti form that are likely to adversely affect the performance of the resulting device [7,8].

The emergence of high-throughput frameworks for first-principles calculations enables the exploration of vast numbers of materials for given applications. This includes studies that screen numerous materials for use in lithium ion batteries [9,10], metal oxides for use as catalysts [11], oxides for transparent conducting oxide applications [12], and stability of the two-dimensional class of materials known as MXenes [13]. Another example of high-throughput screening by Armiento *et al.* studies alternative materials to PZT to determine materials that can accommodate the aforementioned MPB and still maintain desirable piezoelectric properties [14,15].

In this study, the goal is to identify optimal alternative materials for the PZT system that exhibit piezoelectric properties comparable to PZT, and at the same time avoid formation of the undesirable secondary phase when in contact with the Pt electrode. This work builds upon the work of Armiento *et al.* who screened for potential replacements of PZT by looking at the competing phases of their candidate replacements in alloying ratios. We included the added criterion of considering the solution energy of potential alloying elements with the Pt electrode and lattice mismatch of the interface the piezoelectric material forms with the Pt electrode.

II. METHODS

The calculations are performed using density functional theory (DFT) employing the projector-augmented wave method as implemented in the Vienna *ab initio* simulation package (VASP) software [16]. The exchange-correlation functional is approximated using the Perdew-Burke- Ernzerhof (PBE) generalized gradient functional [17], which accurately reproduces solid-state reaction energies [18,19]. Perovskites considered were the cubic $Pm3m$ crystal structure and the tetragonal $P4mm$ crystal structure. We employed a plane-wave cutoff energy of 500 eV and a Monkhorst-Pack *k*-point mesh of $6 \times 6 \times 6$, which was found to converge the energy to within 5 meV/atom.

The high-throughput nature of the study was aided by surveying the Materials Project [20], a database of materials structures and properties calculated using DFT for over 66 000

*Corresponding author: sbs5563@psu.edu

compounds. Structures taken from the Materials Project were reoptimized in our calculations to avoid error from using different parameter settings in the DFT calculations. In particular, the thermodynamic stability calculations rely on structures taken from the Materials Project database and these calculations were carried out by comparing the candidate perovskites with the most stable competing phases that are identified from the Materials Project database. The energy difference between the candidate perovskite and the competing phases determined phase stability, with negative values indicating greater stability. Positive energy differences up to 100 meV/atom were also considered stable, as there is the possibility of stabilization through entropic contributions.

Five screening criteria are considered in this work. The first screening aimed to find *A* and *B* components that do not form any ternary phases with Pt according to the Materials Project. This was a desirable place to start given that one of the motivating factors for this work was to find a replacement for PZT on Pt electrodes that does not suffer from the formation of a secondary alloy phase. The second screening criterion looked to eliminate the candidate perovskites that are metallic since these would not be suitable materials as piezoelectrics. This was done by calculating the electronic structure and eliminating those perovskites with a band gap lower than 0.25 eV. The third screening examined the stability of the perovskites by considering them in a Pt environment and calculating their energy above the convex hull [13]. Those perovskites that showed favorable formation energies in the Pt environment and lacked the formation of secondary Pt-containing phases were considered for further calculations. A cutoff of 100 meV/atom or below was used as entropic contributions could enhance the stability of those with positive energies above the hull. Other reasons for this high value of formation energy is to avoid erroneously removing promising candidates from the pool due to the potentially significant errors in formation energies associated with DFT calculations of oxides. The final screening considerations took into account the lattice mismatch of the candidate perovskites and different alloying compounds with the Pt electrode and the dynamic instabilities of the perovskites. It was desirable for the lattice mismatches to be high for the alloys with the Pt electrode while low for the candidate perovskites with the Pt electrode to favor the growth of the perovskite and not the formation of the secondary phase. Favorable dynamic instabilities for the ferroelectric distortion can be exhibited in perovskite structures, which are desirable for the given application of piezoelectric performance and are a goal of this work.

III. RESULTS

The first screening criterion was conducted without the use of DFT calculations, but rather by searching through the Materials Project database for perovskites with *A*- and *B*-site atom combinations that do not readily form compounds with Pt according to available ternary phase diagrams within the Materials Project. This search was aided with the use of PYMATGEN [21], an open-source python library that allows for ready analysis of data within the Materials Project database. The search included the elements lithium through bismuth, excluding the noble gases and lanthanides. This exercise gave 1572 candidate perovskites for further consideration. Many of the candidates passing this screening contained transition metal *B* sites and alkali and alkaline-earth metal *A* sites.

The second screening criterion was focused on calculating the band gaps of the candidate perovskites to eliminate those that are metallic. Materials with a PBE band gap greater than or equal to 0.25 eV were retained for further consideration, in a manner similar to that of Armiento *et al.* Figure 1 illustrates the calculated band gaps as a function of composition of both the *A* and *B* sites for both cubic and tetragonal perovskite structures. This figure indicates that transition metals such as Ti, Ta, and Zr are common at the *B* site while alkaline earth metals such as Ba and Sc are common on the *A* site for candidate perovskites that satisfy the screening criterion. The calculated band gaps here compare only qualitatively with experiments, which is no surprise as band gaps calculated using the general-gradient approximation commonly underestimate experimental values. For example, cubic $BaZrO_3$ exhibits a

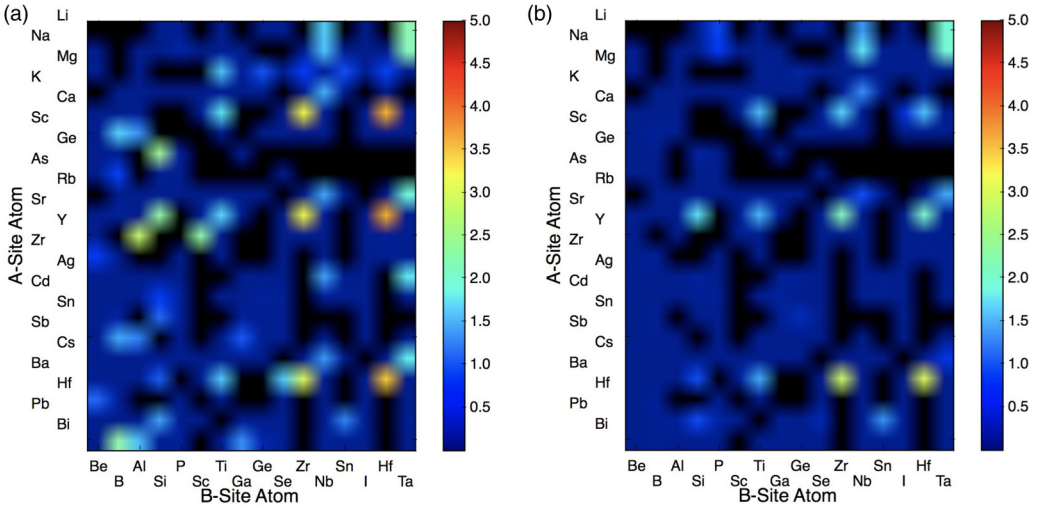

FIG. 1. Band-gap values for *A* sites versus *B* sites for (a) cubic perovskite structures and (b) tetragonal perovskite structures. Black indicates the band gap was not calculated due to the *A* site and *B* site combination failing to meet the first screening criterion.

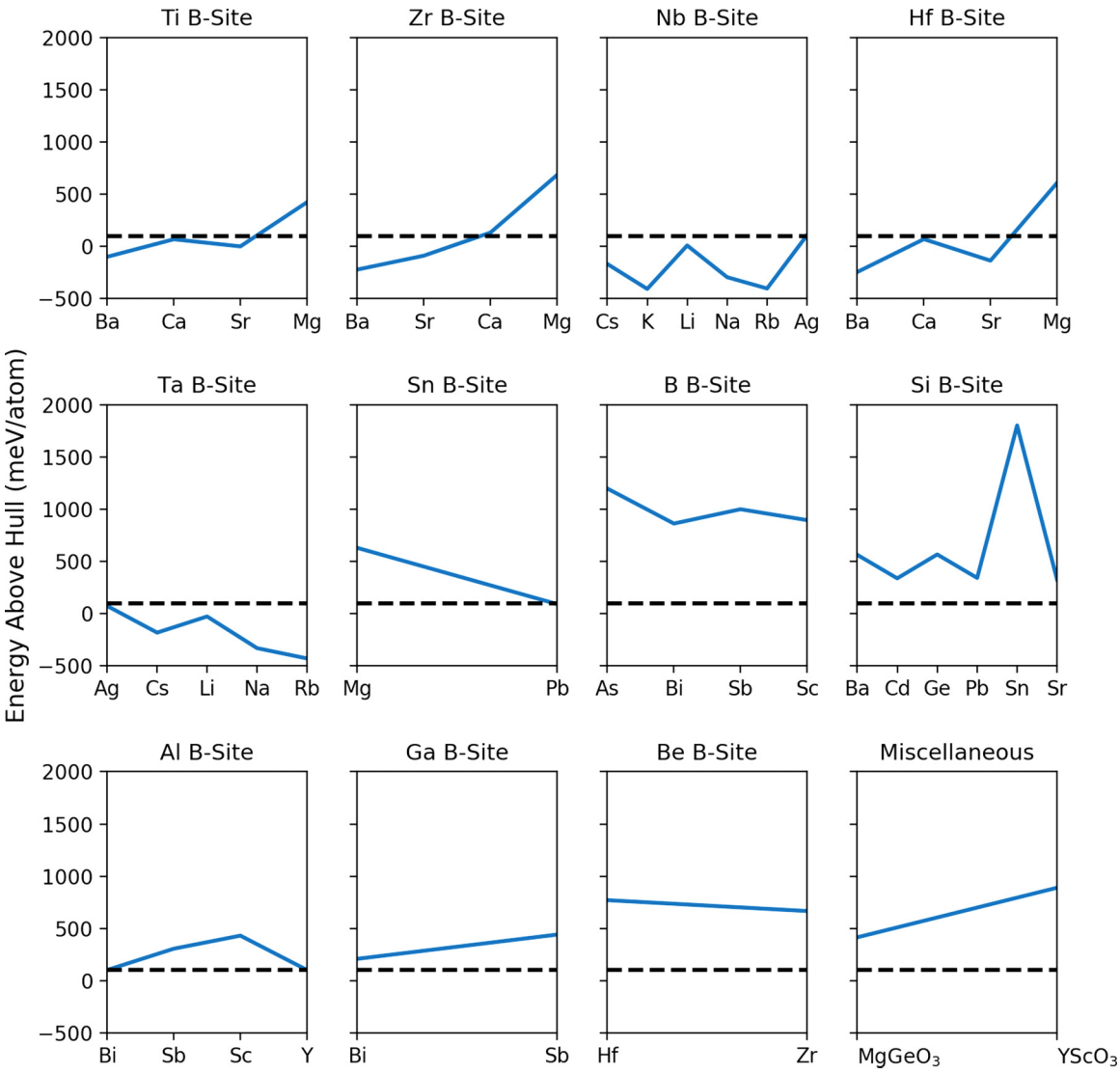

FIG. 2. Energy above the hull calculations for the 45 candidate perovskites with the Pt electrode that passed the band-gap screening criterion. Each plot represents a specific B-site family with the A site plotted on the x axis. The black dashed line represents the cutoff of 100 meV/atom. Any perovskites above this line were eliminated from further consideration.

calculated band gap of 3.00 eV using the PBE functional versus an experimental band gap of 4.85 eV [22]. Following this screening criterion, 45 cubic candidate perovskites remained for additional consideration along with 24 tetragonal candidate perovskites remain.

The third screening criterion considered the thermodynamic stability of the perovskites in contact with Pt. Specifically, the energy of each candidate perovskite and pure metallic platinum was compared with the most stable alternative phases on the corresponding convex hull within the Materials Project database. If a candidate perovskite had a formation energy above the hull greater than 100 meV/atom, this perovskite was eliminated from further consideration. Additionally, if the candidate perovskite was predicted to form an alloy with Pt, that structure was eliminated from further consideration. The results of these calculations are summarized in Fig. 2 for the cubic perovskites. No plot for the tetragonal structures is included because none of them met the screening criterion of having a formation energy equal to or less than 100 meV/atom. Not surprisingly, commonly used perovskites are predicted to pass this criterion, including $BaTiO_3$ and $CaTiO_3$. The results further indicate that transition metals, such as Zr and Ti, are the most common elements on B sites. In the Supplemental Material [23], Table S-I shows the equations used to calculate the energy above the hull for each compound. One observation is that many of the candidate perovskites in contact with the Pt electrode have the potential to form oxides if in a favorable environment. Upon completion of this screening, 19 candidate perovskites remained for further consideration.

The fourth screening criterion considers the lattice misfit of the candidate perovskites with the Pt electrode. Also calculated was the misfit of potential secondary phases alloyed in the fcc structure of Pt on the Pt electrode. Ratios of the A- or B-site alloying elements with Pt that were considered are 1:1 and 3:1, although it is realized that solid solutions with different ratios may also be possible. The goal is to identify perovskites with low misfit on the Pt electrode and a high misfit of the secondary phases with Pt. The lattice mismatch had a significant impact

TABLE I. Misfit calculations of alloying elements with Pt in a 1:3 ratio.

Compound	Misfit (%)
$AgPt_3$	0.831
$TaPt_3$	0.496
$ZrPt_3$	1.878
$CsPt_3$	9.480
$NbPt_3$	0.683
KPt_3	4.727
$RbPt_3$	7.165
$SrPt_3$	6.191
$BaPt_3$	8.772
$HfPt_3$	1.321
$TiPt_3$	0.678
$CaPt_3$	3.180
$LiPt_3$	2.258
$NaPt_3$	0.266
$PbPt_3$	3.785
$SnPt_3$	2.116

on the formation of the secondary phases and proper growth of the perovskite on the Pt electrode. If a secondary phase forms, it may hinder the growth of the perovskite on that face of Pt. Thus, if the secondary phase has a high misfit with Pt, it will be less likely to grow, allowing the formation of the perovskite on the Pt electrode. The calculations were carried out using MPINTERFACES, a freely available software package that can be used with the PYTHON programming language and excels at interfacial analysis [24]. Tables I and II summarize the misfit of the remaining *A* and *B* elements alloying in a 1:3 and 1:1 ratio with Pt, and Table III summarizes the results of the misfit calculations of the remaining candidate perovskites with Pt.

These findings indicate that perovskites containing both Cs and Ba have a higher misfit of greater than 8% of their secondary phases in both alloying ratios with Pt. For the alloying ratio of 1:1 with Pt, Zr, Cs, Rb, Sr, Ba, Hf, Ca, Pb, and

TABLE II. Misfit calculations of alloying elements with Pt in a 1:1 ratio.

Compound	Misfit (%)
AgPt	0.471
TaPt	0.299
ZrPt	12.586
CsPt	19.941
NbPt	0.372
KPt	4.823
RbPt	16.164
SrPt	31.039
BaPt	27.433
HfPt	20.177
TiPt	0.210
CaPt	19.122
LiPt	3.198
NaPt	1.227
PbPt	19.143
SnPt	16.166

TABLE III. Misfit calculations of perovskites with Pt.

Compound	Misfit (%)	Compound	Misfit (%)
$AgTaO_3$	0.468	$CaTiO_3$	2.043
$CsNbO_3$	4.346	$LiNbO_3$	0.448
$CsTaO_3$	4.061	$LiTaO_3$	0.445
$KNbO_3$	1.337	$PbSnO_3$	3.395
$RbTaO_3$	2.257	$SrTiO_3$	0.670
$SrZrO_3$	5.492	$RbNbO_3$	2.379
$BaHfO_3$	5.379	$SrHfO_3$	4.006
$BaZrO_3$	6.464	$BaTiO_3$	1.522
		$CaHfO_3$	3.179

Sn, all exhibit the higher misfit value that is greater than 8%. The candidate perovskites all exhibit relatively small misfits with Pt with the highest being for $BaZrO_3$ with a 6.5% misfit. Those candidate perovskites that contain the elements listed above that have a higher misfit in either alloying ratio were retained for further consideration. This left thirteen final candidates: $CsNbO_3$, $CsTaO_3$, $RbTaO_3$, $SrZrO_3$, $BaHfO_3$, $BaTiO_3$, $BaZrO_3$, $CaHfO_3$, $CaTiO_3$, $PbSnO_3$, $SrTiO_3$, $RbNbO_3$, and $SrHfO_3$.

The final analysis considered the dynamic instability of the materials. Favorable instabilities can exist in the perovskite structure that can lead to ferroelectricity, and therefore, better piezoelectric performance. The main ferroelectric instability can be seen at the Γ_{15} mode in the phonon spectra [25]. Other instabilities may be associated with the rotation of the oxygen octahedral and will be less favorable for piezoelectric performance. While the Γ_{15} instability shows promise for piezoelectric performance, we note that this is not a guarantee that the corresponding tetragonal structures can be realized without modifications such as doping. These calculations were carried out by first relaxing the given structure using more stringent conditions with geometric optimization ending after the forces on all atoms were less than 1.0×10^{-8} eV/Å. The PHONOPY software was used to generate the phonon spectra from the DFT force constants [26].

Of the final 13 candidate perovskites, five showed favorable ferroelectric distortion: $CsNbO_3$, $CsTaO_3$, $RbTaO_3$, $BaTiO_3$, and $RbNbO_3$. The phonon spectra of these five candidate perovskites are provided in Fig. 3. The presence of $BaTiO_3$ is no surprise, as barium titanate is the prototypical ferroelectric. In this case, Ba shows unfavorable lattice mismatch for both alloying ratios studied, while Ti exhibits a favorable misfit of its secondary phase with Pt in both alloying ratios. These observations, coupled with the fact that $BaTiO_3$ is a well-studied material and has failed to exhibit the same degree of piezoelectric behavior as PZT, with a piezoelectric coefficient of 93.95 pC/N [27] compared to the piezoelectric coefficient of PZT being 180 pC/N [28], makes barium titanate a nonideal replacement for PZT in this particular work.

For those two candidate materials that contain Nb at the *B* site, $CsNbO_3$ and $RbNbO_3$, it is noted that both have the pitfall of having a small misfit for both alloying ratios of the Nb atom. Cs has the higher misfit with the Pt electrode in both 1:1 and 1:3 alloying ratios while Rb is only higher for the 1:1 ratio. Thus $CsNbO_3$ would appear to be the better choice, although

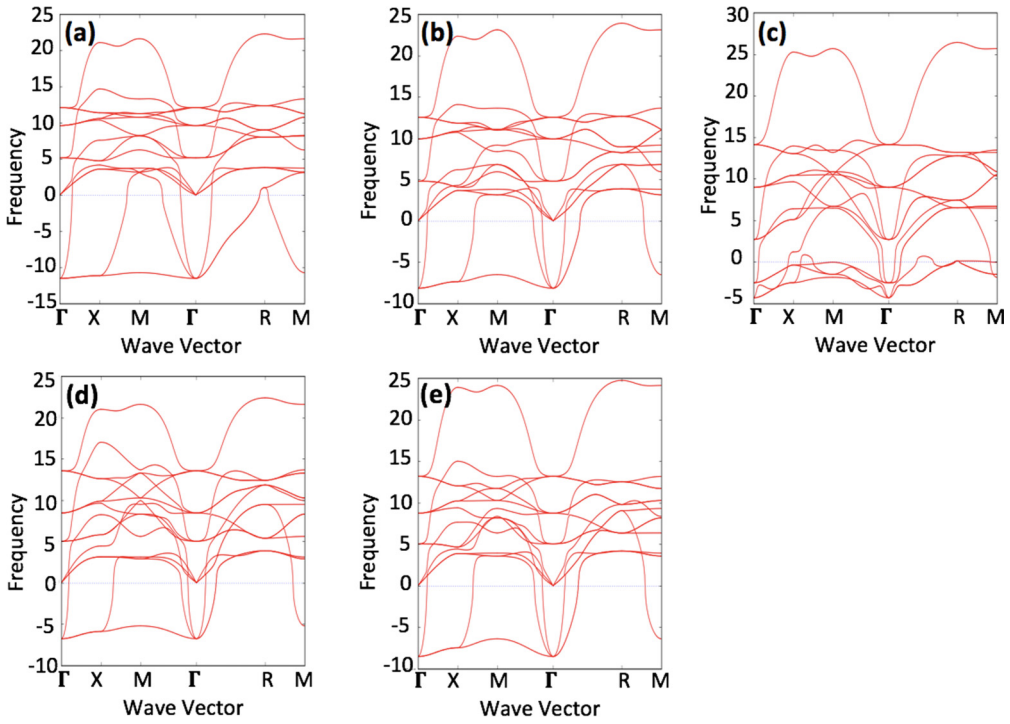

FIG. 3. Phonon spectra of the five candidate perovskites that show the favorable ferroelectric distortion at Γ_{15}, those being (a) $CsNbO_3$, (b) $CsTaO_3$, (c) $RbTaO_3$, (d) $BaTiO_3$, and (e) $RbNbO_3$.

both have the potential of enabling the secondary phase to form on Pt. Previous first-principles studies of $RbNbO_3$ also predict the favorable ferroelectric distortion in the $Pm3m$ structure and additional studies of other crystal structures predict that it will have favorable nonlinear optical and electro-optical properties [29].

Similar findings were found for the Ta B-site candidates of $CsTaO_3$ and $RbTaO_3$ as those with Nb at the B site. The Ta atom shows favorable lattice mismatch with the Pt electrode in both alloying ratios. Previous work also found that $RbTaO_3$ is not expected to show favorable ferroelectric properties due to the ferroelectric instability being suppressed [29]. Thus $CsTaO_3$ would appear to be the better candidate for further exploration.

IV. CONCLUSION

In summary, high-throughput DFT calculations were conducted to search through 1572 perovskite compounds as a replacement for the PZT system, and specifically for a perovskite structure with similar excellent piezoelectric properties as PZT but without the growth of the secondary phases that exist between the PZT and Pt electrode. After screening for band-gap values, thermodynamic stability, lattice mismatch, and ferroelectric properties, we conclude that $RbNbO_3$, $CsNbO_3$, and $CsTaO_3$ are desirable replacement materials for PZT and worthy of further investigation.

ACKNOWLEDGMENTS

The authors thank Tao Liang for many helpful discussions. J.A.B. acknowledges support by a National Science Foundation (NSF) Graduate Research Fellowship (Grant No. DGE1255832) and training was provided by the NSF (Grant No. DGE-1449785). R.G.H. acknowledges NSF support (Grant No. ACI-1440547), as do F.-Y.L., M.A., and S.B.S. (Grants No. DMR-1207293 and No. DMR-1056587). Computational resources were provided by the University of Florida's High Performance Computing clusters and the Advanced CyberInfrastructure provided by The Institute for CyberScience at The Pennsylvania State University (http://ics.psu.edu).

[1] M. T. Ghoneim, M. A. Zidan, M. Y. Alnassar, A. N. Hanna, J. Kosel, K. N. Salama, and M. M. Hussain, Adv. Electron. Mater. **1**, 1500045 (2015).
[2] F. Kurokawa, M. Kishimoto, Y. Tsujiura, H. Hida, and I. Kanno, Microsyst. Technol. **22**, 1275 (2016).
[3] J. H. Park and S. K. Joo, Appl. Phys. Lett. **108**, 103504 (2016).
[4] W. Xu, H.-L. Huang, Y. Liu, C. Luo, G. Z. Cao, and I. Y. Shen, Sens. Actuators, A **246**, 102 (2016).
[5] F. Cordero, Materials **8**, 8195 (2015).
[6] C. A. Randall, N. Kim, J. P. Kucera, W. Cao, and T. R. Shrout, J. Am. Ceram. Soc. **81**, 677 (1998).
[7] J. L. Jones, J. M. LeBeau, J. Nikkel, A. A. Oni, J. H. Dycus, C. Cozzan, F. Y. Lin, A. Chernatynskiy, J. C. Nino, S. B. Sinnott, S. Mhin, G. L. Brennecka, and J. Ihlefeld, Adv. Mater. Interfaces **2**, 1500181 (2015).
[8] F.-Y. Lin, A. Chernatynskiy, J. Nikkel, R. Bulanadi, J. L. Jones, J. C. Nino, and S. B. Sinnott, J. Am. Ceram. Soc. **99**, 356 (2016).

[9] A. Jain, G. Hautier, S. P. Ong, S. Dacek, and G. Ceder, Phys. Chem. Chem. Phys. **17**, 5942 (2015).
[10] S. Sun, Y. Chen, and J. Yu, J. Phys. Chem. C **119**, 25770 (2015).
[11] J. M. Kweun, C. Li, Y. Zheng, M. Cho, Y. Y. Kim, and K. Cho, Appl. Surf. Sci. **370**, 279 (2016).
[12] N. Sarmadian, R. Saniz, B. Partoens, D. Lamoen, K. Volety, G. Huyberechts, and J. Paul, Phys. Chem. Chem. Phys. **16**, 17724 (2014).
[13] M. Ashton, K. Mathew, R. G. Hennig, and S. B. Sinnott, J. Phys. Chem. C **120**, 3550 (2016).
[14] R. Armiento, B. Kozinsky, M. Fornari, and G. Ceder, Phys. Rev. B **84**, 014103 (2011).
[15] R. Armiento, B. Kozinsky, G. Hautier, M. Fornari, and G. Ceder, Phys. Rev. B **89**, 134103 (2014).
[16] G. Kresse and J. Furthmüller, Phys. Rev. B **54**, 11169 (1996).
[17] J. P. Perdew, K. Burke, and M. Ernzerhof, Phys. Rev. Lett. **77**, 3865 (1996).
[18] M. Fishman, H. L. Zhuang, K. Mathew, W. Dirschka, and R. G. Hennig, Phys. Rev. B **87**, 245402 (2013).
[19] S. Kurth, J. P. Perdew, and P. Blaha, Int. J. Quantum Chem. **75**, 889 (1999).
[20] A. Jain, S. P. Ong, G. Hautier, W. Chen, W. D. Richards, S. Dacek, S. Cholia, D. Gunter, D. Skinner, G. Ceder, and K. A. Persson, APL Mater. **1**, 011002 (2013).
[21] S. P. Ong, W. D. Richards, A. Jain, G. Hautier, M. Kocher, S. Cholia, D. Gunter, V. L. Chevrier, K. A. Persson, and G. Ceder, Comput. Mater. Sci. **68**, 314 (2013).
[22] L. S. Cavalcante, V. M. Longo, M. Zampieri, J. W. M. Espinosa, and P. S. Pizani, J. Appl. Phys. **103**, 063527 (2008).
[23] See Supplemental Material at http://link.aps.org/supplemental/10.1103/PhysRevMaterials.2.025002 for thermodynamic stability calculation values.
[24] K. Mathew, A. K. Singh, J. J. Gabriel, K. Choudhary, S. B. Sinnott, A. V. Davydov, F. Tavazza, and R. G. Hennig, Comput. Mater. Sci. **122**, 183 (2016).
[25] A. I. Lebedev, Phys. Solid State **51**, 362 (2009).
[26] A. Togo and I. Tanaka, Scr. Mater. **108**, 1 (2015).
[27] M. Zgonik, P. Bernasconi, M. Duelli, R. Schlesser, P. Günter, M. H. Garrett, D. Rytz, Y. Zhu, and X. Wu, Phys. Rev. B **50**, 5941 (1994).
[28] G.-T. Park, J.-J. Choi, J. Ryu, H. Fan, and H.-E. Kim, Appl. Phys. Lett. **80**, 4606 (2002).
[29] A. I. Lebedev, Phys. Solid State **57**, 331 (2015).